Intronic elements associated with insomnia and restless legs syndrome exhibit cell-type-specific epigenetic features contributing to *MEIS1* regulation

Daniel D. Lam [ORCID][1,2,†], Ana Antic Nikolic[1,2,†], Chen Zhao[1,2,†], Nazanin Mirza-Schreiber[1], Wojciech Krężel[3,4,5,6],

Konrad Oexle[1,2] and Juliane Winkelmann[1,2,7,8,*]

[1]Institute of Neurogenomics, Helmholtz Center Munich, German Research Center for Environmental Health, Neuherberg 85764, Germany
[2]Institute of Human Genetics, Klinikum rechts der Isar, School of Medicine, Technical University of Munich, Munich 81675, Germany
[3]Institut de Génétique et de Biologie Moléculaire et Cellulaire, Illkirch 67400, France
[4]Institut de la Santé et de la Recherche Médicale, U964, Illkirch 67400, France
[5]Centre National de la Recherche Scientifique, UMR 7104, Illkirch 67404, France
[6]Université de Strasbourg, Illkirch, France
[7]Chair of Neurogenetics, Klinikum rechts der Isar, School of Medicine, Technical University of Munich, Munich 81675, Germany
[8]Munich Cluster for Systems Neurology (SyNergy), Munich, Germany
*To whom correspondence should be addressed at: Institute of Neurogenomics, Helmholtz Center Munich, Ingolstädter Landstraße 1, 85764 Neuherberg, Germany. Tel: +49 (0)8931871884; Fax: +49 (0)8931873297; Email: juliane.winkelmann@tum.de

[†]Equal contribution.

Abstract

A highly evolutionarily conserved myeloid ecotropic viral integration site 1 (*MEIS1*) intronic region is strongly associated with restless legs syndrome (RLS) and insomnia. To understand its regulatory function, we dissected the region by analyzing chromatin accessibility, enhancer-promoter contacts, DNA methylation and expression quantitative trait locus (eQTLs) in different human neural cell types and tissues. We observed specific activity with respect to cell type and developmental maturation, indicating a prominent role for distinct highly conserved intronic elements in forebrain inhibitory neuron differentiation. Two elements were hypomethylated in neural cells with higher *MEIS1* expression, suggesting a role of enhancer demethylation in gene regulation. *MEIS1* eQTLs showed a striking modular chromosomal distribution, with forebrain eQTLs clustering in intron 8/9. Clustered regularly interspersed short palindromic repeats interference targeting of individual elements in this region attenuated *MEIS1* expression, revealing a complex regulatory interplay of distinct elements. In summary, we found that *MEIS1* regulation is organized in a modular pattern. Disease-associated intronic regulatory elements control *MEIS1* expression with cell type and maturation stage specificity, particularly in the inhibitory neuron lineage. The precise spatiotemporal activity of these elements likely contributes to the pathogenesis of insomnia and RLS.

Introduction

A series of genome-wide association studies (GWAS) consistently identify strong association signals for restless legs syndrome (RLS), a common neurological disorder, in introns 7–9 of the myeloid ecotropic viral integration site 1 (*MEIS1*) locus (1–3). A recent series of GWAS for insomnia, sleep and circadian traits also identify strong association signals in this same region, due to a combination of phenotypic overlap with RLS and, arguably, pleiotropic effects (4–8). The lead single nucleotide polymorphism (SNP) for both RLS and insomnia is rs113851554, and the others signals are largely concordant (see Fig. 1).

MEIS1 encodes a homeodomain-containing transcription factor of the three amino acid loop extension (TALE) superclass (9). MEIS proteins are broadly expressed in embryonic development and regulate diverse developmental processes, including limb and vascular patterning, eye and neural development, hematopoiesis and

cardiogenesis (9). The scope of these diverse roles in disparate tissues necessitates precise spatiotemporal regulation of *MEIS1* expression. Such precision is typically conferred by arrayed non-coding regulatory elements (10,11).

Indeed, the *MEIS1* locus harbors an array of highly evolutionarily conserved non-coding elements with presumed regulatory function. Our previous work has shown that one *MEIS1* intronic variant, rs12469063, affects enhancer activity in the developing forebrain (12), but it was not clear if this effect was mediated via regulation of *MEIS1* expression. Here, we interrogated tissue and cell-type-specific chromatin accessibility, promoter-enhancer contacts and DNA methylation as readouts of functional activity using cultured human cells. We show that several elements in the disease-associated intronic region are active in forebrain neural development, particularly in the inhibitory neuron lineage, with activity
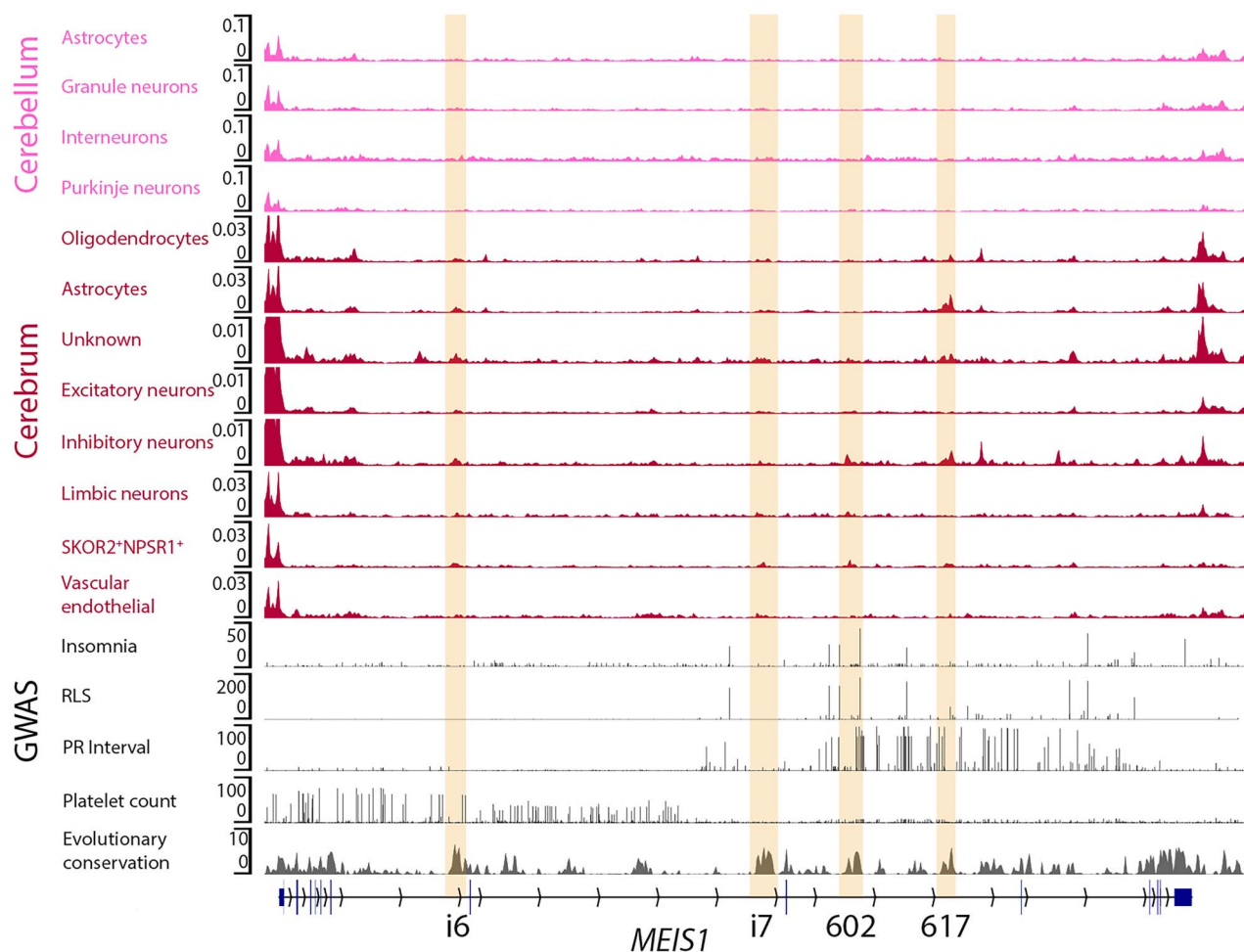
Figure 1. Chromatin accessibility in human brain cell types. Aggregated single cell ATAC-seq read density in 12 fetal human brain cell types. Data from (14). GWAS data (scale $-\log_{10}$P) are from (1,4,60,61). Evolutionary conservation is phyloP 100-way (62). Elements in intron 6 (i6), 7 (i7) and 8 (602 and 617) are highlighted.

peaking during the late neurogenic period. Clustered regularly interspersed short palindromic repeats (CRISPR) interference experiments revealed distributed regulation of *MEIS1* transcription by multiple elements. Thus, intronic elements tightly control *MEIS1* expression in forebrain development, particularly in the inhibitory neuron lineage, and variants within them can impact forebrain development and function *via* transcriptional regulation.

Results
Human cell-type-specific accessibility of *MEIS1* intronic elements

The accessibility of chromatin is considered to reflect its regulatory capacity (13). Leveraging a recently published atlas of human fetal chromatin accessibility (14), we assessed the *MEIS1* locus in 12 annotated cell types of the cerebellum and cerebrum (telencephalon or forebrain). We observed pronounced cell-type specificity of chromatin accessibility, with greatest accessibility of several elements, including those previously designated 602 and 617 (12), in inhibitory neurons of the cerebrum (Fig. 1).

Having identified the greater accessibility of intronic *MEIS1* elements in forebrain inhibitory neurons, we

sought to further characterize the regulatory landscape of the *MEIS1* locus by implementing *in vitro* differentiation of human induced pluripotent stem cells (iPSC) towards forebrain inhibitory neurons. Forebrain inhibitory neurons are generated in the ganglionic eminences (GEs), transient fetal structures with a well-described architecture (15). GEs are the source of striatal (caudate/putamen) cells, which migrate radially towards the striatum as they mature and differentiate, as well as cortical interneurons, which migrate radially and then tangentially towards the cortex (15). In this differentiation paradigm, adapted from (16), pluripotent stem cells first undergo neural induction towards a forebrain identity, delineated by *FOXG1* and *PAX6* expression (17,18), then ventralization towards a GE identity, characterized by *NKX2-1* and *GSX2* expression [(19,20); Fig. 2].

Developmental dynamics of chromatin accessibility in the human *MEIS1* locus

To characterize the developmental dynamics of *MEIS1* regulation, we assayed chromatin accessibility using assay for transposase-accessible chromatin using sequencing (ATAC-seq) at three stages of *in vitro* differentiation
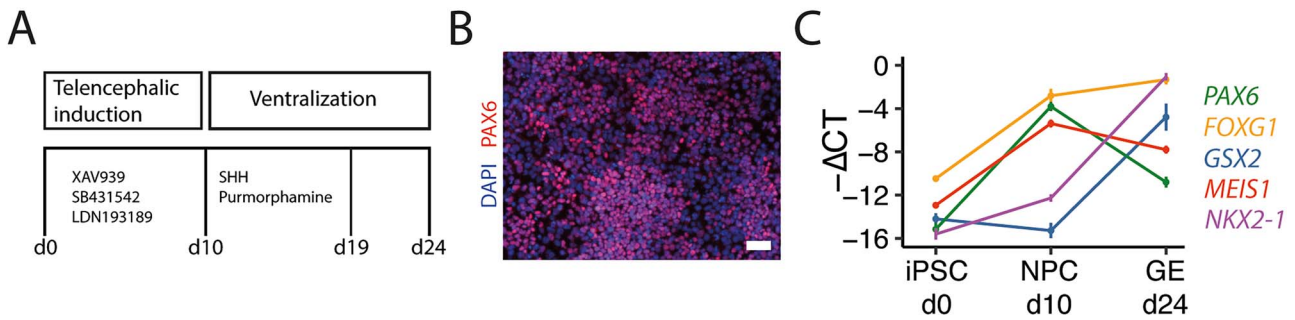
Figure 2. *In vitro* ganglionic eminence differentiation. (**A**) *In vitro* ganglionic eminence differentiation scheme. (**B**) Successful *in vitro* neural induction at day 10 shown by PAX6 expression (red). Scale bar, 50 μm. (**C**) Expression of key marker genes through differentiation. Values are -(C_T of marker gene—C_T of *GAPDH* internal reference) and displayed as mean ± SD of 5–6 replicates per stage. C_T, PCR cycles to threshold.

in human cells: iPSC, neural progenitor cells (NPC) and GE-like cells. We observed changes in accessibility at distinct elements during differentiation (Fig. 3), such as a progressive increase in accessibility of the 617 element and a transient increase in accessibility in an intron 7 element (i7). We also performed ATAC-seq on three commercially available neural cell lines, neural stem cells (NSCs), inhibitory neurons (γ-aminobutyric acid [GABA] neurons) and excitatory glutamatergic neurons. Here too we observed cell-type-specific accessibility patterns (Fig. 3). Of note, the 602 element (12), carrying the lead SNP for RLS association, was only accessible in GABA neurons (Fig. 3). Concordantly, the 602 element was accessible in neural tissue enriched in GABA neurons (fetal lateral GE and putamen, Fig. 3), but not in non-neural cells and tissues where MEIS1 nevertheless has an important function (Fig. 3). An intron 6 element (i6) was also selectively accessible in GABA neurons and NSCs (Fig. 3). Taken together, these results demonstrate selective accessibility of intronic elements in the *MEIS1* locus across different tissues, cell types and developmental stages.

Developmental dynamics of chromatin accessibility in the murine *Meis1* locus

In the developing mouse, *Meis1* expression in diverse tissues (limbs, eye, blood and brain) peaks around mid-gestation (21–24). This is also true of chromatin accessibility (Supplementary Material, Fig. S2). Moreover, each tissue shows a unique pattern of chromatin accessibility within the *Meis1* locus, with the 617 and 602 elements in particular showing selective accessibility in forebrain and the i6 element showing selective brain activity (Fig. 4A, Supplementary Material, Fig. S2). Of note, chromatin immunoprecipitation sequencing (ChIP-seq) analysis at approximately the same embryonic stage revealed that both the 617 and 602 elements are bound by DLX2, a key transcription factor for forebrain GABA neuron differentiation [(25); Fig. 4A]. Analysis of the temporal dynamics of chromatin accessibility in developing mouse forebrain single nucleus ATAC-seq data support the selective role of element 617 in the inhibitory neuron trajectory (Fig. 4B–D).

MEIS1 enhancer-promoter contacts

Non-coding regulatory elements regulate transcription by establishing direct contacts with gene promoters *via* chromosomal conformational changes (26). Intronic elements do not necessarily regulate their host gene, because they can interact topologically with other promoters (27). To determine the topological interactions of the human *MEIS1* promoter, we performed circular chromosome conformation capture followed by sequencing [4C-seq; (28,29)] in five cell types: iPSCs, NPC, GE cells, glutamatergic neurons and GABAergic neurons (Fig. 5). In all cell types, a gene-spanning contact was detected (Fig. 5), presumably denoting a stable topologically associating domain (TAD; (30)]. In contrast, interaction of element 617 and an additional intron 8 element with the *MEIS1* promoter only reached statistical significance in cell types of the inhibitory neuron trajectory (Fig. 5). The interactions corresponded with the accessibility of intronic elements, in accordance with the functional relatedness of chromatin accessibility and intrachromosomal contacts (13). Supporting our findings, a recently published analysis of cell-type-specific chromosome conformation in the developing human cortex (31) reveals an array of interactions between the *MEIS1* promoter and intronic elements, particularly in radial glia and inhibitory neurons (Supplementary Material, Fig. S4).

Regulation of *MEIS1* expression by enhancer demethylation

To determine the relationship between enhancer methylation and *MEIS1* expression, we characterized methylation using a microarray approach in three cell types: iPSCs, NPC differentiated from iPSCs with fibroblast growth factor (NPC-FGF) and commercially available NSCs. Neural cells expressed *MEIS1*, whereas iPSCs had negligible expression (relative to NSCs, mean ± SEM [standard error of the mean]: iPSCs, 0.5 ± 0.02; NSCs 100 ± 3; NPC-FGF 1467 ± 27; Fig. 6A). Across the locus, *MEIS1*-expressing neural cells (NSCs and NPCs) had slightly higher levels of methylation than iPSCs. In contrast, elements 617 and i6 were strongly hypomethylated in neural cells (Fig. 6B; cg06919693 within 617, NSC vs
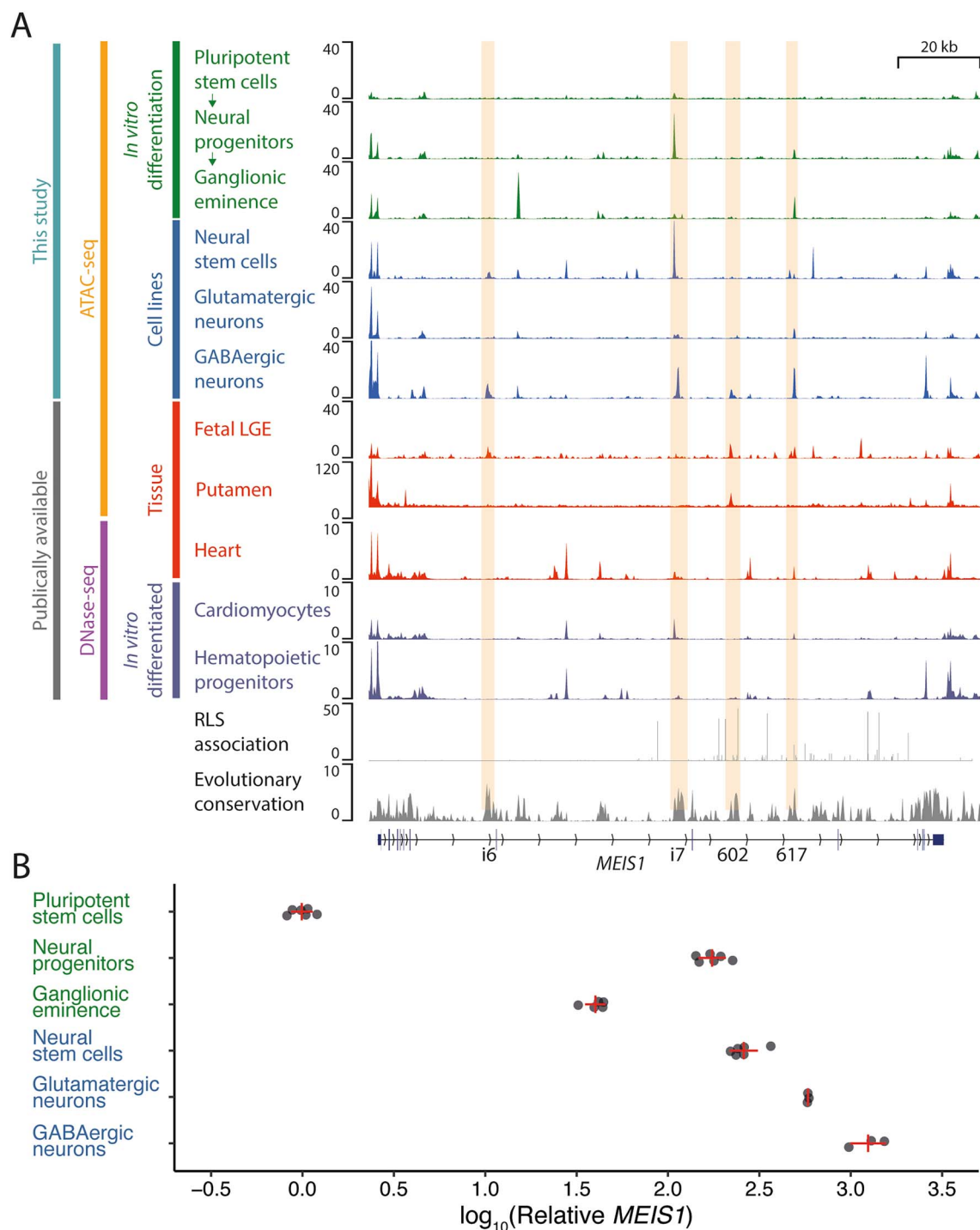
Figure 3. Developmental dynamics of chromatin accessibility in the human *MEIS1* locus. (**A**) ATAC-seq (-log$_{10}$P values) and DNase-seq (read depth-normalized signal) of *in vitro* differentiated cells, commercially available cell lines and tissues. Fetal LGE is 19th gestational week data from (63). Putamen data are from BOCA (64). Heart, cardiomyocyte and hematopoietic progenitor data are from ENCODE (65,66). RLS association is from unpublished metaGWAS, scale is -log$_{10}$P. Evolutionary conservation is phyloP 100-way (62). (**B**) Relative *MEIS1* expression in the first 6 cell lines depicted in A determined by RT-qPCR, expressed relative to pluripotent stem cells (=1). Plotted are mean ± SD. The mean expression values ± standard error are: neural progenitors 176 ± 31; ganglionic eminence 40 ± 5; neural stem cells 263 ± 52; glutamatergic neurons 584 ± 6; GABAergic neurons 1265 ± 277. *n* = 3–6 replicates per cell line.

iPSC $P_{adj} = 6.2 \times 10^{-13}$, NPC-FGF vs iPSC $P_{adj} = 1.3 \times 10^{-12}$; 6 CpGs within i6, NSC vs iPSC $P = 2.1 \times 10^{-24}$, NPC-FGF vs iPSC $P = 2.9 \times 10^{-47}$). We also compared our results to published whole genome bisulfite sequencing results at multiple stages of isogenic *in vitro* neural differentiation,

with broadly similar results (Supplementary Material, Fig. S5). Specifically, the previously published studies (32,33) found moderate demethylation of *MEIS1* intronic elements i6, i7 and 617, particularly at later stages of differentiation (Supplementary Material, Fig. S5).
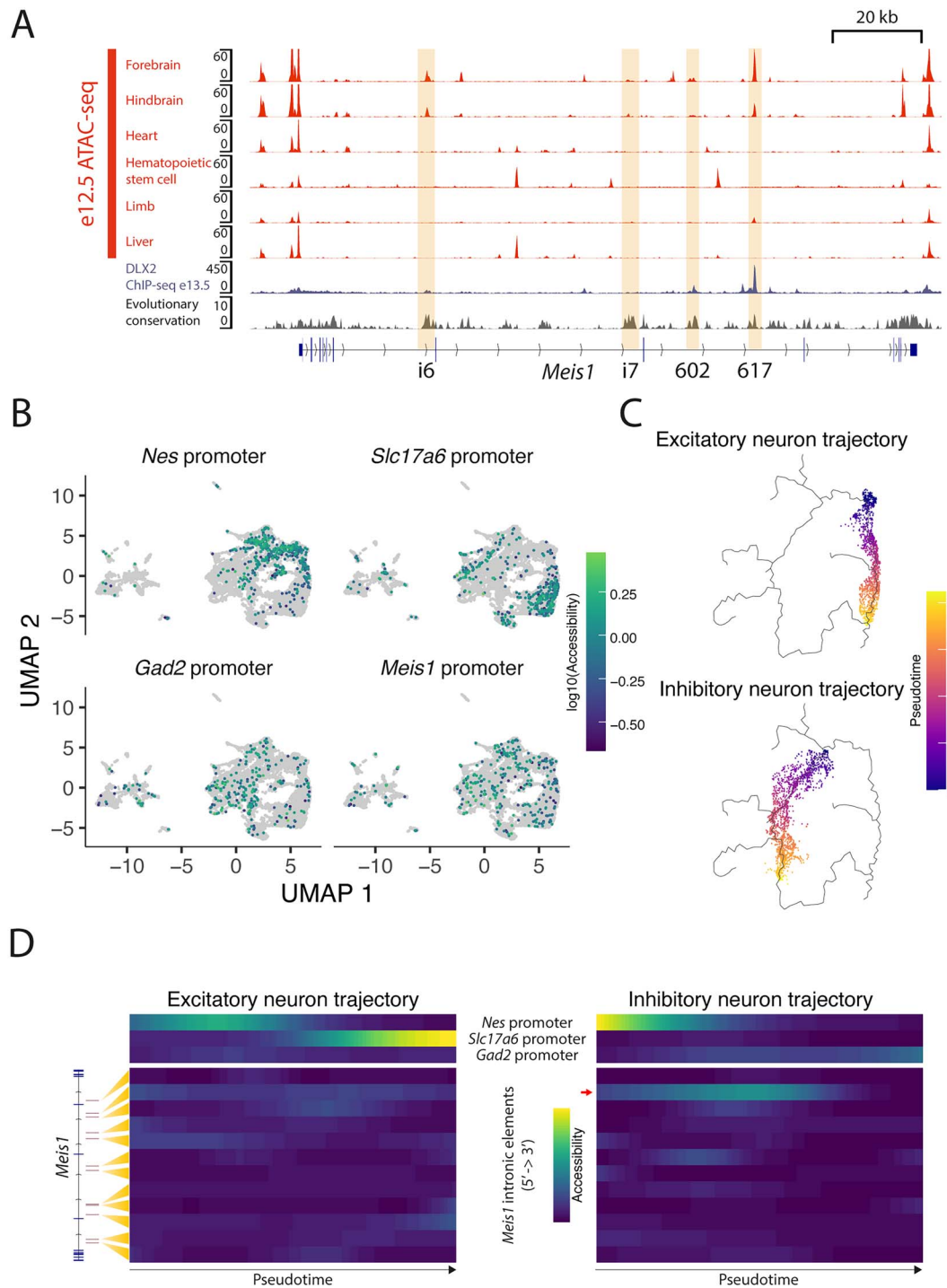
Figure 4. Chromatin accessibility in the murine *Meis1* locus. (**A**) ATAC-seq -log$_{10}$P values for 2 replicates of different tissues of embryonic day 12.5 (e12.5) mouse embryos [data from (65,66)]; ganglionic eminence DLX2 ChIP-seq at e13.5 [data from (67)]; and evolutionary conservation (phyloP 60-way) in the murine *Meis1* locus, shown here inverted (5′ → 3′) to compare with the human locus. (**B**) Accessibility of promoters for *Nes* (denotes progenitor cells), *Slc17a6* (denotes excitatory neurons), *Gad2* (denotes inhibitory neurons) and *Meis1* in 15 767 single nuclei from developing mouse brain (data from (51)]. (**C**) Pseudotemporal ordering on uniform manifold approximation and projection coordinates of developing mouse forebrain single nucleus ATAC-seq data in the excitatory (1484 nuclei) and inhibitory neuron (1834 nuclei) trajectories. (**D**) Pseudotemporal accessibility profiles of three reference promoters and 12 *Meis1* intronic sites in the excitatory and inhibitory neuron trajectories. Element 617 in the inhibitory neuron trajectory is highlighted with a red arrow.

MEIS1 expression quantitative trait loci

Harnessing large-scale genotype- and tissue-specific gene expression data from GTEx (34), we inspected expression quantitative trait locus (eQTLs) of *MEIS1* expression. eQTLs for different tissues and cell types occurred at vast linear chromosomal distances from the *MEIS1* gene body (extending to ∼550 kb 5′ and ∼830 kb 3′). The eQTLs showed a distinctive tissue-
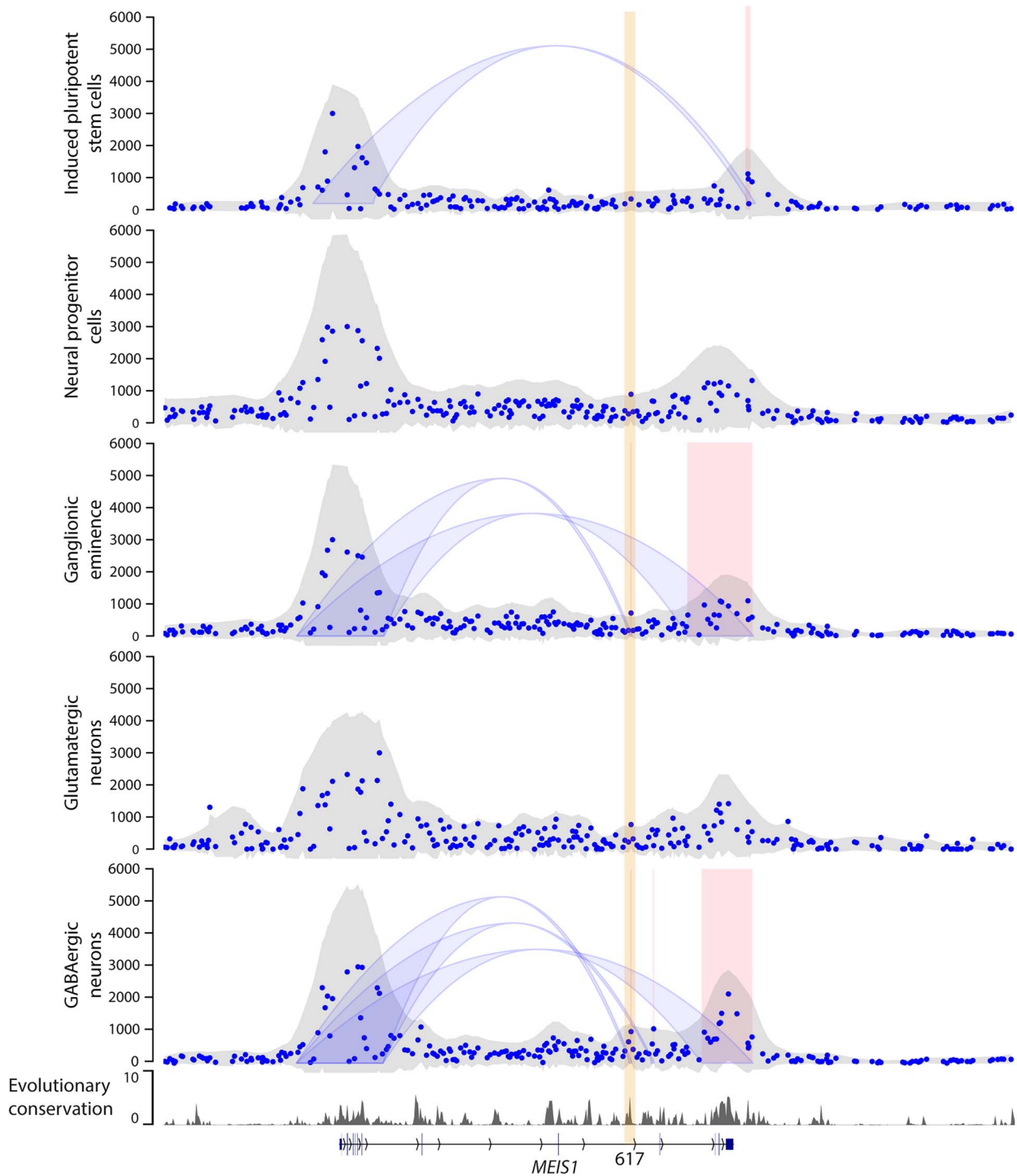
Figure 5. Topological conformation of the *MEIS1* locus. (**A**) 4C-seq counts and statistically significant (FDR < 0.01) interactions (blue arcs & red rectangles) in human pluripotent cells, neural progenitor cells, ganglionic eminence-like cells, glutamatergic neurons and GABAergic neurons. Evolutionary conservation is phyloP 100-way.

specific distribution, with for example amygdala eQTLs clustering distally 5′ to the gene, cerebellum, tibial nerve, and fibroblast eQTLs distally 3′ to the gene, and lung eQTLs proximally 5′ to and within the gene (Fig. 7A). Of note, caudate and cortex eQTLs clustered in intron 8 and 9, including within elements 602 and 617 (Fig. 7B). As the GEs give rise to both caudate (part of the striatum)

and cortex, these eQTLs likely relate to effects of intron 8/9 variants that persist through development and into adulthood in cells of the GE lineage. The effect sizes also reflect the proportion of GE-derived GABAergic neurons. Effect sizes in caudate [80–90% of neurons GE-derived GABAergic (35,36)] were consistently larger than cortex [~25% of neurons GE-derived GABAergic (37)].
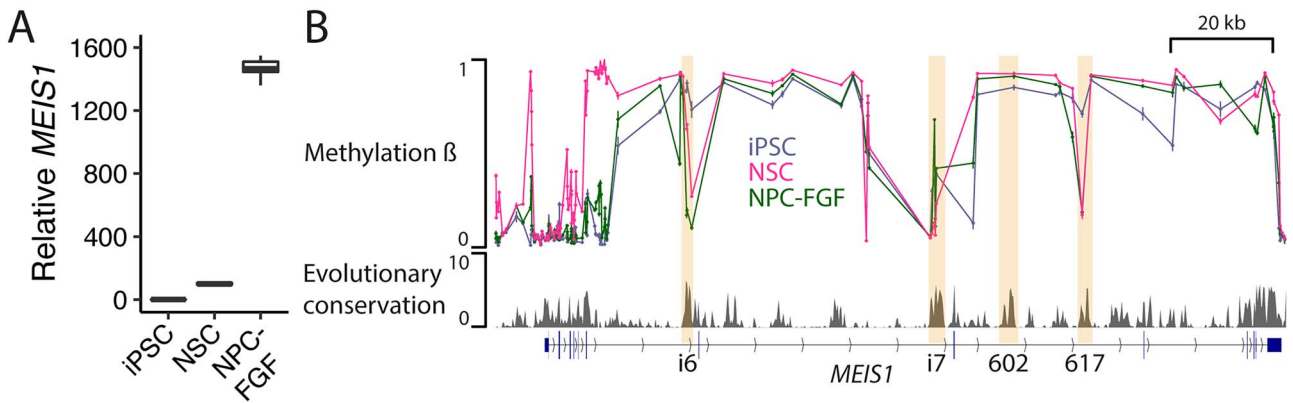
Figure 6. DNA methylation in the *MEIS1* locus. (**A**) *MEIS1* expression by qPCR in induced pluripotent stem cells (iPSC), neural stem cells (NSC) and iPSC-derived neural progenitor cells (NPC-FGF). Expression is relative to NSCs (=100) shown as boxplots (*n* = 6 per cell type). (**B**) Methylation β values for 123 CpG sites within the *MEIS1* locus for the three cell types (*n* = 6 per cell type). Plotted are mean ± SEM. Also shown is evolutionary conservation (phyloP 100-way).
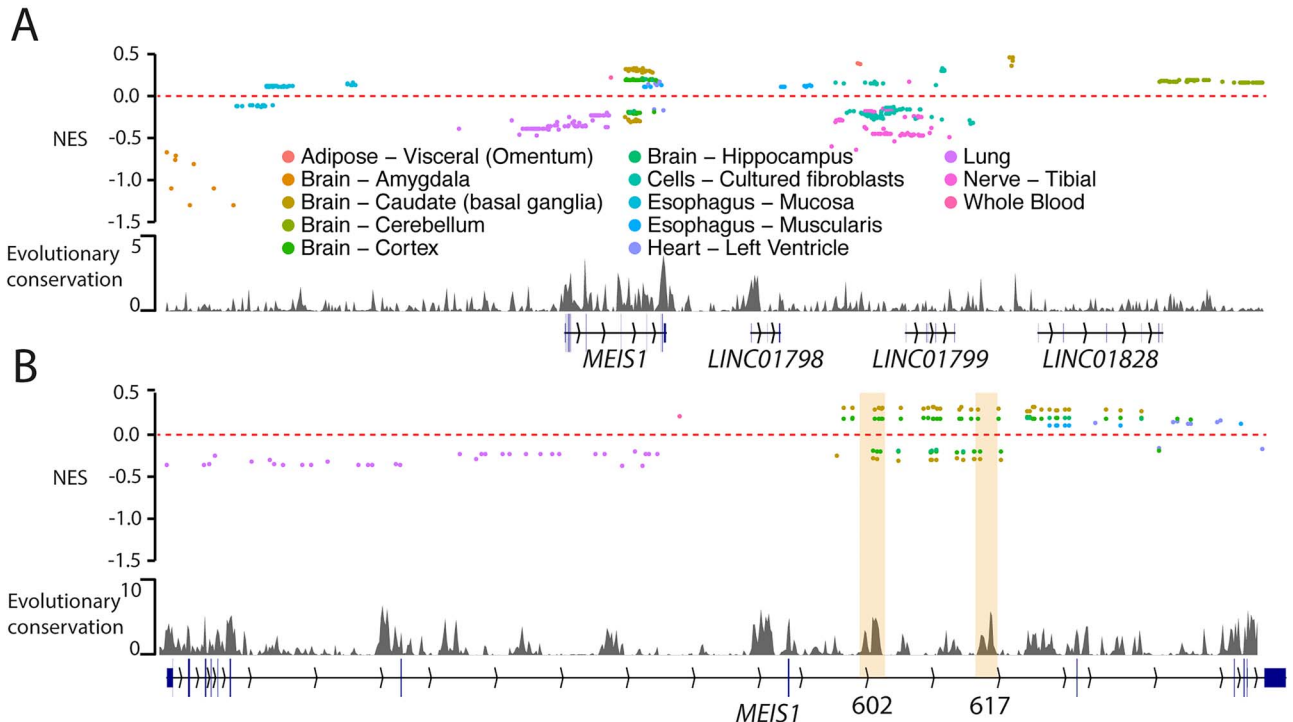

Figure 7. MEIS1 eQTLs. (**A**) All 533 *MEIS1* eQTLs from 13 tissues plotted by genomic position and normalized effect size (NES). Evolutionary conservation (phyloP 100-way) is also shown. (**B**) 157 *MEIS1* eQTLs mapping within the *MEIS1* locus. The data are identical to A at higher genomic resolution.

Overall, *MEIS1* eQTLs show a remarkable tissue-specific segregation within and beyond the locus.

CRISPR interference of intronic *MEIS1* elements reveals regulatory interplay

Several intronic *MEIS1* elements show epigenetic features characteristic of regulatory elements, including chromatin accessibility, contacts with the *MEIS1* promoter, differential methylation and eQTL effects. However, direct evidence of enhancer activity depends on observing transcriptional effects of functional perturbation. We used CRISPR interference (38–40) to interrogate the functional contribution of three elements to *MEIS1*

expression in NSCs. We observed an effect of suppression of the intron 7, 602 and 617 elements on *MEIS1* transcription, with a magnitude similar to targeting the *MEIS1* promoter (20–30% suppression of transcription; Fig. 8). Thus, in human NSCs, these three elements are all involved in regulating *MEIS1* expression, supporting *MEIS1* transcription to a similar extent.

Discussion

The strong association and comparatively strong effect size of intronic *MEIS1* variants with sleep-related phenotypes [e.g. $P = 2 \times 10^{-180}$ and odds ratio, OR = 1.92 for
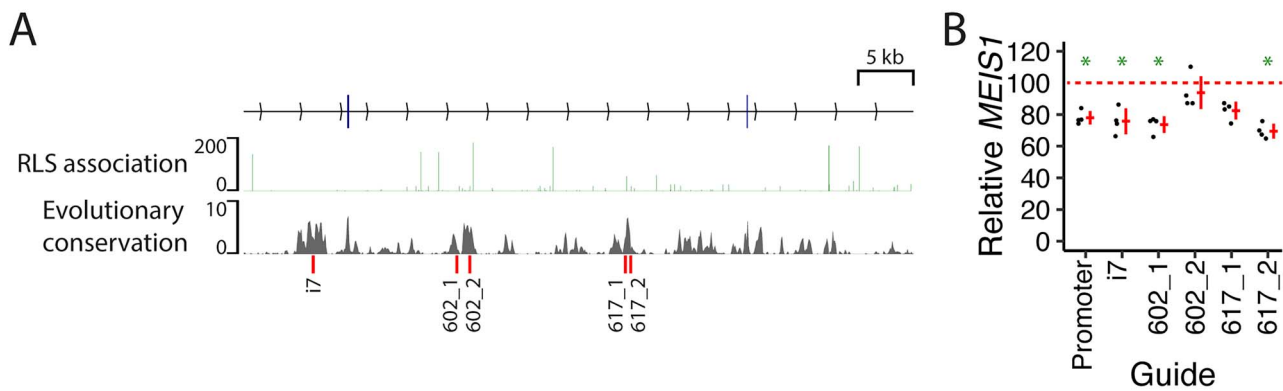
Figure 8. CRISPR interference of intronic *MEIS1* elements. (**A**) Genomic location of CRISPR guide target sites (red lines, bottom). Also shown are RLS association (scale is -log₁₀P) and evolutionary conservation (phyloP 100-way). (**B**) *MEIS1* qPCR from NSCs subjected to CRISPR interference with the indicated guides, relative to a *UBQLN2* promoter guide ($n = 4$ replicates per guide). $*P < 0.05$, one-sided *t*-test compared with *UBQLN2* promoter guide.

Table 1. Functional evidence by element and assay

Element	Human ATAC-seq	Mouse ATAC-seq	4C-seq	Methylation	CRISPRi
i6	✓	✓	×	✓	Nd
i7	✓	×	×	×	✓
602	✓	✓	×	×	✓
617	✓	✓	✓	✓	✓

rs113851554 in RLS metaGWAS (1)] indicate a prominent role for this non-coding region in the development of these traits. In this study, we functionally dissected this region to better understand its regulatory function.

We found that specific intronic elements have specific activity, inferred from accessibility, topology and methylation, with respect to cell types, maturation stage and differentiation lineage (Table 1). In particular, element 617 showed a transient peak in activity corresponding to late neurogenesis, and 602 showed persistent activity, particularly in the GABAergic lineage. Element 602 appeared highly selective to this lineage, whereas element 617 also showed some activity in the cardiogenic and limb development context. In agreement with a particularly important role for elements 617 and 602 in GABAergic differentiation, both are bound by DLX2, a key transcription factor for forebrain GABA neuron differentiation (25). Elements i7 and i6 were also active in the GABA neuron lineage to differing degrees of specificity.

There was high concordance of *MEIS1* intronic element accessibility and enhancer-promoter contact frequency in proliferating neural cells, in agreement with the prevailing view that formation of enhancer-promoter contacts and increased enhancer accessibility are mutually reinforcing and functionally related (13,26). The enhancer activity corresponding to a maturation stage when cells are transitioning from mitotic to post-mitotic corresponds with the known role of MEIS1 in regulating the cell cycle and balance between proliferation and differentiation (9). The interactions between the *MEIS1*

promoter and intronic elements in neural development, particularly in the inhibitory neuron lineage, reinforce the importance of *MEIS1* and its regulatory elements in this context.

We also found that neural cells expressing *MEIS1* tended to have higher DNA methylation across the *MEIS1* locus, except at elements 617 and i6. As DNA methylation, and enhancer methylation specifically, typically exert repressive effects on transcription *via* effects on transcription factor binding (41–43), we infer that hypomethylation of these elements is permissive for *MEIS1* transcription. Pluripotent cells differentiating into neural cells undergo broad changes in DNA methylation, with demethylation predominating over hypermethylation as genes and regulatory elements supporting differentiation become activated (32,33). Indeed, regions becoming demethylated during neural differentiation are enriched for enhancers near induced genes and their methylation levels are inversely correlated with expression of the nearest gene (32,33). Thus, enhancer demethylation may be an important mechanism of *MEIS1* regulation by facilitating transcription factor binding.

As indicated by eQTL results, the regulation of *MEIS1* in different tissues and cell types is organized in a modular fashion, with regulatory elements for specific tissues clustered in distinct genomic compartments. eQTLs for forebrain tissues cluster clearly within intron 8/9, where the association with sleep-related phenotypes is strongest.

Finally, we show that epigenetic suppression of elements i7, 602 and 617 by targeted CRISPR interference attenuates *MEIS1* expression to a similar extent as suppression of the *MEIS1* promoter in human neural cells. Thus, we assume that each of these elements contributes to a similar extent to the promoter in supporting *MEIS1* transcription. Future combinatorial suppression experiments may provide insight into the extent of synergism between these elements, whereas suppression experiments in different cell types would enhance understanding of their cell-type-specific roles.

In summary, the introns of *MEIS1* are scattered with apparent regulatory elements. Their organization into distinct modules appears to underlie the rich pleiotropy of the gene, with related but distinct functions in diverse tissues and developmental stages. One such module, mostly within intron 8 but extending to neighboring introns, is prominently associated with sleep/wake-related phenotypes including RLS and insomnia. Here, we show that distinct elements within this module are selectively engaged during differentiation of inhibitory neurons, exerting temporally specific enhancer effects. Genetic variation in *MEIS1* intronic elements probably tunes inhibitory neuron differentiation, thus underlying the association with sleep/wake-related phenotypes.

Materials and Methods
Cell lines

The HMGU1 and HMGU12 iPSC lines were obtained from the Helmholtz Center Munich iPSC Core Facility. The lines were generated from the BJ (ATCC CRL-2522) line of foreskin fibroblasts from a healthy newborn human male donor by transfection of six mRNA reprogramming factors (*OCT4*, *SOX2*, *KLF4*, *LIN28*, *MYC*, *NANOG*; StemRNA-NM Reprogramming Kit, Stemgent). Cells were maintained in mTeSR culture media (STEMCELL Technologies, #85850) on cell culture dishes (Sigma, #CLS3516-50EA) coated with Matrigel (Corning, #354277) or Geltrex (ThermoFisher Scientific, #A1413202).

Human NSCs derived from H9 (WA09) human embryonic stem cells were purchased from ThermoFisher Scientific (#N7800200). The cells were cultured in complete StemPro NSC SFM (ThermoFisher Scientific #A1050901) consisting of KnockOut D-MEM/F-12 with StemPro Neural Supplement, EGF, bFGF and GlutaMAX on Geltrex-coated cell culture dishes.

GABAergic neurons and glutamatergic neurons (iCell GABANeurons Kit, #01279 and iCell GlutaNeurons Kit, #01279) were purchased from Cellular Dynamics. iCell GABANeurons and GlutaNeurons are highly pure populations of human neurons, comprised primarily of GABAergic and cortical glutamatergic neurons respectively, derived from induced pluripotent stem (iPS) cells using proprietary differentiation and purification methods. Cells were collected for downstream experiments 5 days post-plating.

In vitro differentiation

iPSCs were differentiated towards GE using the protocol from Close *et al.* (16) with slight modifications. iPSCs were grown to 90% confluence and then dissociated with TrypLE Select Enzyme (ThermoFisher Scientific, #12604013) for 5 min at 37°C. 500 000 iPS cells were plated per well of a 24 well plate in mTeSR supplemented with RevitaCell (ThermoFisher Scientific, #A2644501). The next day (day 1), the medium was replaced with neural induction medium (NIM) consisting of DMEM/F12 (Thermo Fisher Scientific,

#11320074), N-2 (ThermoFisher Scientific, #17502048), B-27 (ThermoFisher Scientific, #17504044) and Gluta-MAX supplement (ThermoFisher Scientific, #35050061), MEM non-essential amino acids (ThermoFisher Scientific, #11140035), 0.11 mM 2-mercaptoethanol (ThermoFisher Scientific, #31350010), 0.05% (v/v) Bovine Serum Albumin Fraction V Solution (ThermoFisher Scientific, #15260037), Penicillin–Streptomycin (ThermoFisher Scientific, #15140122) (all Thermo Fisher), 100 nM (LDN193189 Biomol, #Cay11802-1) and 10 μM SB431542 (Cayman Chemical, #13031-5) and 2 μM XAV939 (R & D Systems, #3748/10). NIM was changed daily until day 5, when it was replaced with 75% NIM/25% N2 medium [DMEM/F12, N-2 supplement, 0.15% (w/v) dextrose, 55 μM 2-mercaptoethanol, Penicillin–Streptomycin]. On day 7, cells were fed with 50% NIM/50% N2, and on day 9 with 25% NIM/75% N2. On day 10, cells were dissociated into a single cell suspension with TrypLE Express Enzyme and plated onto Matrigel-coated 24-well plates in 25% NIM/75% N2 supplemented with RevitaCell at 2 million cells per well. At this stage some material was harvested for RNA extraction and ATAC-seq (NPC stage). On day 11 the medium was replaced with N2/B27 medium (N2 medium with B-27 supplement) containing 0.65 μM purmorphamine (Cayman Chemical). On days 19–23, cells were fed daily with N2/B27 medium without purmorphamine. On day 24, cells were collected for RNA extraction and ATAC-seq.

To generate NPC-FGF cells used for DNA methylation studies, the protocol from Reinhardt *et al.* (44) was used. iPSCs were dissociated with 2 mg/ml collagenase IV ThermoFisher Scientific, #17104019 for 45 min at 37°C, which was then neutralized with mTeSR. The cells were centrifuged at 200 g for 4 min, then resuspended in differentiation medium (20% KnockOut Serum Replacement (ThermoFisher Scientific, #10828010) and MEM Non-Essential Amino Acids (ThermoFisher Scientific, #11140050) in DMEM-F12) supplemented with a small molecule cocktail (1 μM dorsomorphin, 10 μM SB431542, 3 μM CHIR99021 and 0.5 μM purmorphamine) and RevitaCell, and grown in ultra-low attachment plates to form embryoid bodies. The medium was replaced the following day (day 2). On day 3, the medium was changed to N2B27 medium (DMEM-F12 and Neurobasal 1:1, B-27 and N-2 supplements and GlutaMAX) with the small molecule cocktail. The medium was changed on day 4, and on day 5 without purmorphamine and CHIR99021. On day 6, embryoid bodies were plated on Geltrex-coated plates in N2B27 medium with dorsomorphin, SB431542, and basic fibroblast growth factor (bFGF, 10 ng/ml). This medium was replaced daily. Cells were propagated for 3 passages after Matrigel plating, then harvested at confluence.

ATAC-seq

We used the previously described protocol of Buenrostro *et al.* (45) with 50 000 cells per replicate. Adherent cells were dissociated with TrypLE Select Enzyme and

centrifuged at 500 *g* for 5 min at 4°C. The cell pellet was resuspended in ice-cold lysis buffer (10 mM Tris–HCl, pH 7.4, 10 mM NaCl, 3 mM MgCl$_2$ and 0.1% IGEPAL CA-630) and centrifuged for 20 min at 500 *g* at 4°C. The pellet was resuspended in transposition reaction mix (Nextera Tn5 transposase, (Illumina, #FC-121-1030)) and incubated for 30 min at 37°C. Samples were purified using the MinElute Kit (Qiagen, #28004).

Purified samples were then amplified by polymerase chain reaction (PCR; maximum 12 cycles) using barcoded primers from the Nextera Index Kit (Illumina, #FC-121-1011). To determine the optimal number of cycles for each sample, samples were first amplified for 5 cycles (5 min at 72°C, 30 s at 98°C, and 5 cycles of 10 s at 98°C, 30 s at 63°C and 1 min at 72°C). Samples amplified for 5 cycles were then subjected to qPCR (SYBR Green, ThermoFisher Scientific, #S7567) . The additional number of cycles required was the number of cycles required to reach one quarter of the maximal fluorescence intensity in the first 5 cycles. The remainder of each sample was subsequently amplified for an additional 5–7 cycles.

Amplified samples were purified with SPRI (Solid Phase Reversible Immobilization) beads (Beckam Coulter, #A63880) at a ratio 1:1.8 sample:beads, and fragment size was checked using the High Sensitivity DNA kit (Agilent). Libraries were sequenced on a HiSeq 4000 (Illumina), two samples per lane, 100 bp paired end reads. Reads were trimmed and aligned with bowtie2 (46), with standard parameters and a maximum fragment length of 2000. Duplicate reads were removed with Picard. De-duplicated reads were filtered for high quality [samtools (47), MAPQ ≥30], non-mitochondrial chromosome, non-Y chromosome and proper pairing (samtools flag 0 × 2). Peaks were called with macs2 (48), and filtered out with IDR threshold of 0.1 (49) and blacklist of artifactual regions in hg19. Libraries were quality controlled by downsampling to 5 million reads and evaluating transcription start site enrichment (RefSeq) and fraction of reads in peaks. Data were visualized with pyGenomeTracks (50).

Single nucleus ATAC-seq analysis

Single nucleus ATAC-seq data from developing mouse forebrain (51) were downloaded from GEO (accession GSE100033). Data were processed with Cicero (52) using default parameters. The trajectory root was chosen manually based on accessibility of the *Nes* promoter.

4C-seq

We used the previously described protocol of van de Werken *et al.* (53). Cells were dissociated to single cells with TrypLE Express and fixed in 2% formaldehyde in Dulbecco's phosphate-buffered saline (DPBS) (ThermoFisher Scientific, #14190144) for 10 min. Glycine was added to a final concentration of 222 mM to quench the cross-linking reaction. Cells were centrifuged for 10 min at 400 *g* at 4°C, the supernatant discarded and the cell pellet resuspended in cold lysis buffer (50 mM Tris pH 7.5, 150 mM NaCl, 5 mM EDTA, 0.5% NP-40, 1% Triton

X-100, cOmplete protease inhibitor cocktail, Roche with 1× Complete Mini EDTA free proteinase inhibitor (Roche #11245200)) and incubated on ice for 30 min. To ensure complete lysis, cells were stained with methyl green pyronin (Dianova, #MGP125). In the case of efficient lysis, nuclei are stained blue and cytoplasm pink. Next, lysed cells were centrifuged and the pellet was washed with DPBS and resuspended in water. NEBuffer and SDS (0.3% final concentration) were added and the samples were incubated at 37°C for 1 h while shaking at 900 rpm with occasional pipetting to break cell aggregates. Triton X-100 Sigma, #T8532 was added to a concentration of 2.5% and samples were again incubated at 37°C for 1 h while shaking.

The first round of digestion was done with DpnII (New England Biolabs) at 37°C overnight. Digest efficiency was checked on an agarose gel. DpnII was inactivated by incubating for 20 min at 65°C. Ligation was performed with T4 ligase (Thermo Fisher) overnight at 16°C and checked on an agarose gel. Samples were then decrosslinked with Proteinase K at 65°C overnight. After DNA purification with phenol-chloroform, the second round of digestion was performed with Csp6I (Thermo Fisher). Digestion was followed by overnight ligation with T4 ligase at 16°C. Samples were purified using Amicon Ultra-15 columns (Millipore, #UFC900324) and DNA quantified using the Qubit dsDNA HS Assay Kit (ThermoFisher Scientific, #Q32851).

To generate 4C libraries, we used 3.2 μg of DNA for PCR amplification divided into 16 PCR reactions, using the Expand Long Template PCR System (Sigma Aldrich, #11681834001). PCR primers were designed using the *MEIS1* promoter as a viewpoint and included Truseq adapters. Primer genomic targets are shown in Supplementary Material, Fig. S3 and sequences in Supplementary Material, Table S1. PCR conditions were 2 min at 94°C, 30 cycles of 15 s at 94°C, 1 min at 55°C and 3 min at (68)°C followed by 5 min at (68)°C. Pooled libraries were purified using SPRI beads (Beckam Coulter, #A63880) at a ratio of 1:1.8 sample:beads, and fragment size was checked using the High Sensitivity DNA kit (Agilent, #5067-4626). The libraries were sequenced on an Illumina MiSeq. Reads were trimmed with Trimmomatic v0.36 (54), aligned with bowtie2 (46) and subsequently processed, filtered, analyzed and visualized according to Basic4Cseq (55) in R v 4.0.2.

DNA methylation analysis

Genome-wide DNA methylation from iPSCs, NSCs and iPSC-derived neural progenitor cells (NPC-FGF) was assessed using the Infinium Human Methylation EPIC BeadChip (Illumina), according to the manufacturer's protocol. The EPIC array covers over 850 000 methylation sites. Genome-wide raw signal intensity data were subjected to a standard quality control (QC) and quantile normalization pipeline using the minfi (56) and limma (57) packages in R v 4.0.2. Probes with poor quality (<95% call rate or detection *P* value > 0.01), SNPs at the CpG site

and cross-reactivity were filtered out prior to differential methylation analysis. Methylation level for each CpG site was calculated as a beta value $\beta = M/(M + U + 100)$, where $M > 0$ and $U > 0$ denote the methylated and unmethylated signal intensities measured by the array and the offset of 100 is added to $M + U$ to stabilize beta values when both M and U are small. Beta values range between 0 and 1, with 0 indicating no methylation and 1 full methylation. CpG sites were classified as hypo- or hypermethylated according to ENCODE guidelines. Probe-wise and region-wise differential methylation between the different cell types were estimated using M values in limma, obtaining moderated t-statistics, P values and adjusted P values using false discovery rate (FDR) for each CpG site.

eQTL analysis

MEIS1 eQTL data were downloaded from GTEx (34) and plotted with ggplot2 (58) and pyGenomeTracks (59).

CRISPR interference

To prepare CRISPRi lentiviruses, Lenti-X™ 293 T Cells (Takara) were seeded on 10-cm dishes (6×10^6 cells per dish). The next day, cells were transfected with second generation lentiviral packaging plasmids (pMD2.G, 0.72 pmol; and psPAX2, 1.3 pmol) and the CRISPRi transfer plasmid (pLV hU6-sgRNA hUbC-dCas9-KRAB-T2a-Puro, 1.64 pmol) carrying the respective guide RNA (see Supplementary Material, Table S1). pMD2.G was a gift from Didier Trono (Addgene plasmid # 12 259; http://n2t.net/addgene:12 259; RRID:Addgene_12 259). psPAX2 was a gift from Didier Trono (Addgene plasmid # 12 260; http://n2t.net/addgene:12 260; RRID:Addgene_12 260). pLV hU6-sgRNA hUbC-dCas9-KRAB-T2a-Puro was a gift from Charles Gersbach (Addgene plasmid # 71 236; http://n2t.net/addgene:71 236; RRID:Addgene_71 236). Plasmids were mixed with 48-μg polyethylenimine 'Max', MW 40 000 Da (Polysciences) in 600 μl OptiMEM (ThermoFisherScientific, #1985062), incubated for 20 min at room temperature, then added to the Lenti-X cells. Cells were incubated at 37°C for 16 h, then medium was changed. Forty-eight hours later, the medium was harvested, centrifuged at 1200 $\times$ g for 5 min at 4°C and filtered through a 0.45 μm polyethersulfone (PES) syringe filter. The filtered supernatant was used to transduce NSCs.

NSCs were seeded in Geltrex-coated 24-well plates (50 000 cells per well). The following day, CRISPRi lentiviral supernatants (100 μl per well) were added. Two days later, cells were selected with puromycin (1 μg/ml) for 24 h, after which the medium was replaced without puromycin. RNA was harvested the following day (see section 'Quantitative PCR').

Quantitative PCR

Total RNA was extracted with the RNeasy Mini Kit (Qiagen, #74104). RNA was reverse transcribed into complementary DNA (cDNA) using the High-Capacity cDNA Reverse Transcription Kit (ThermoFisher Scientific, #4368814). Quantitative PCR was performed in duplicate using TaqMan Universal PCR Master Mix (ThermoFisher Scientific, #4304437) with TaqMan gene expression assays: *MEIS1* (Hs00180020_m1), *PAX6* (Hs00240871_m1), *FOXG1* (Hs01850784_s1), *GSX2* (Hs00370195_m1), *NKX2-1* (Hs00968940_m1) and *GAPDH* (Hs02758991_g). qPCR reactions were performed on a 7900HT Fast Real-Time PCR System (Applied Biosystems) as follows: 2 min at 50°C, 10 min at 95°C, and 40 cycles of 15 s at 95°C and 1 min at 60°C. For quantification, the $2^{-\Delta\Delta CT}$ method was used with *GAPDH* as the endogenous reference.

Supplementary Material

Supplementary Material is available at *HMG* online.

Author's contributions

D.D.L. and A.A.N. designed the study and analyzed the data. A.A.N. performed the experiments. D.D.L. wrote the manuscript and prepared the figures with input from all authors. C.Z. and N.M.-S. performed bioinformatic analysis. W.K. and J.W. supervised the project. All authors read and approved the final manuscript.

References

1. Schormair, B., Zhao, C., Bell, S., Tilch, E., Salminen, A.V., Pütz, B., Dauvilliers, Y., Stefani, A., Högl, B., Poewe, W. *et al.* (2017) Identification of novel risk loci for restless legs syndrome in genome-wide association studies in individuals of European ancestry: a meta-analysis. *Lancet Neurol.*, **16**, 898–907.

2. Winkelmann, J., Czamara, D., Schormair, B., Knauf, F., Schulte, E.C., Trenkwalder, C., Dauvilliers, Y., Polo, O., Högl, B., Berger, K. *et al.* (2011) Genome-wide association study identifies novel restless legs syndrome susceptibility loci on 2p14 and 16q12.1. *PLoS Genet.*, **7**, e1002171.

3. Winkelmann, J., Schormair, B., Lichtner, P., Ripke, S., Xiong, L., Jalilzadeh, S., Fulda, S., Pütz, B., Eckstein, G., Hauk, S. *et al.* (2007) Genome-wide association study of restless legs syndrome identifies common variants in three genomic regions. *Nat. Genet.*, **39**, 1000–1006.

4. Lane, J.M., Jones, S.E., Dashti, H.S., Wood, A.R., Aragam, K.G., van Hees, V.T., Strand, L.B., Winsvold, B.S., Wang, H., Bowden, J. *et al.* (2019) Biological and clinical insights from genetics of insomnia symptoms. *Nat. Genet.*, **51**, 387–393.

5. Jones, S.E., Lane, J.M., Wood, A.R., van Hees, V.T., Tyrrell, J., Beaumont, R.N., Jeffries, A.R., Dashti, H.S., Hillsdon, M., Ruth, K.S. *et al.* (2019) Genome-wide association analyses of chronotype in 697,828 individuals provides insights into circadian rhythms. *Nat. Commun.*, **10**, 343.

6. Lane, J.M., Liang, J., Vlasac, I., Anderson, S.G., Bechtold, D.A., Bowden, J., Emsley, R., Gill, S., Little, M.A., Luik, A.I. *et al.* (2017) Genome-wide association analyses of sleep disturbance traits identify new loci and highlight shared genetics with neuropsychiatric and metabolic traits. *Nat. Genet.*, **49**, 274–281.

7. Jansen, P.R., Watanabe, K., Stringer, S., Skene, N., Bryois, J., Hammerschlag, A.R., de Leeuw, C.A., Benjamins, J.S., Muñoz-Manchado, A.B., Nagel, M. *et al.* (2019) Genome-wide analysis of insomnia in 1,331,010 individuals identifies new risk loci and functional pathways. *Nat. Genet.*, **51**, 394–403.

8. Hammerschlag, A.R., Stringer, S., de Leeuw, C.A., Sniekers, S., Taskesen, E., Watanabe, K., Blanken, T.F., Dekker, K., Te Lindert, B.H.W., Wassing, R. *et al.* (2017) Genome-wide association analysis of insomnia complaints identifies risk genes and genetic overlap with psychiatric and metabolic traits. *Nat. Genet.*, **49**, 1584–1592.

9. Schulte, D. and Geerts, D. (2019) MEIS transcription factors in development and disease. *Development*, **146**.

10. Pennacchio, L.A., Ahituv, N., Moses, A.M., Prabhakar, S., Nobrega, M.A., Shoukry, M., Minovitsky, S., Dubchak, I., Holt, A., Lewis, K.D. *et al.* (2006) In vivo enhancer analysis of human conserved non-coding sequences. *Nature*, **444**, 499–502.

11. Nord, A.S., Blow, M.J., Attanasio, C., Akiyama, J.A., Holt, A., Hosseini, R., Phouanenavong, S., Plajzer-Frick, I., Shoukry, M., Afzal, V. *et al.* (2013) Rapid and pervasive changes in genome-wide enhancer usage during mammalian development. *Cell*, **155**, 1521–1531.

12. Spieler, D., Kaffe, M., Knauf, F., Bessa, J., Tena, J.J., Giesert, F., Schormair, B., Tilch, E., Lee, H., Horsch, M. *et al.* (2014) Restless legs syndrome-associated intronic common variant in Meis1 alters enhancer function in the developing telencephalon. *Genome Res.*, **24**, 592–603.

13. Klemm, S.L., Shipony, Z. and Greenleaf, W.J. (2019) Chromatin accessibility and the regulatory epigenome. *Nat. Rev. Genet.*, **20**, 207–220.

14. Domcke, S., Hill, A.J., Daza, R.M., Cao, J., O'Day, D.R., Pliner, H.A., Aldinger, K.A., Pokholok, D., Zhang, F., Milbank, J.H. *et al.* (2020) A human cell atlas of fetal chromatin accessibility. *Science*, **370**.

15. Marín, O. and Rubenstein, J.L.R. (2001) A long, remarkable journey: tangential migration in the telencephalon. *Nat. Rev. Neurosci.*, **2**, 780–790.

16. Close, J.L., Yao, Z., Levi, B.P., Miller, J.A., Bakken, T.E., Menon, V., Ting, J.T., Wall, A., Krostag, A.-R., Thomsen, E.R. *et al.* (2017) Single-cell profiling of an in vitro model of human interneuron development reveals temporal dynamics of cell type production and maturation. *Neuron*, **93**, 1035–1048.e5.

17. Stoykova, A., Treichel, D., Hallonet, M. and Gruss, P. (2000) Pax6 modulates the Dorsoventral patterning of the mammalian telencephalon. *J. Neurosci.*, **20**, 8042–8050.

18. Martynoga, B., Morrison, H., Price, D.J. and Mason, J.O. (2005) Foxg1 is required for specification of ventral telencephalon and region-specific regulation of dorsal telencephalic precursor proliferation and apoptosis. *Dev. Biol.*, **283**, 113–127.

19. Sussel, L., Marin, O., Kimura, S. and Rubenstein, J.L. (1999) Loss of Nkx2.1 homeobox gene function results in a ventral to dorsal molecular respecification within the basal telencephalon: evidence for a transformation of the pallidum into the striatum. *Development*, **126**, 3359–3370.

20. Corbin, J.G., Gaiano, N., Machold, R.P., Langston, A. and Fishell, G. (2000) The Gsh2 homeodomain gene controls multiple aspects of telencephalic development. *Development*, **127**, 5007–5020.

21. Mercader, N., Leonardo, E., Azpiazu, N., Serrano, A., Morata, G., Martínez-A, C. and Torres, M. (1999) Conserved regulation of proximodistal limb axis development by Meis1/Hth. *Nature*, **402**, 425–429.

22. Heine, P., Dohle, E., Bumsted-O'Brien, K., Engelkamp, D. and Schulte, D. (2008) Evidence for an evolutionary conserved role of homothorax/Meis1/2 during vertebrate retina development. *Development*, **135**, 805–811.

23. Pineault, N., Helgason, C.D., Lawrence, H.J. and Humphries, R.K. (2002) Differential expression of Hox, Meis1, and Pbx1 genes in primitive cells throughout murine hematopoietic ontogeny. *Exp. Hematol.*, **30**, 49–57.

24. Toresson, H., Parmar, M. and Campbell, K. (2000) Expression of Meis and Pbx genes and their protein products in the developing telencephalon: implications for regional differentiation. *Mech. Dev.*, **94**, 183–187.

25. Panganiban, G. and Rubenstein, J.L.R. (2002) Developmental functions of the distal-less/dlx homeobox genes. *Development*, **129**, 4371–4386.

26. Schoenfelder, S. and Fraser, P. (2019) Long-range enhancer–promoter contacts in gene expression control. *Nat. Rev. Genet.*, **20**, 437–455.

27. Smemo, S., Tena, J.J., Kim, K.-H., Gamazon, E.R., Sakabe, N.J., Gómez-Marín, C., Aneas, I., Credidio, F.L., Sobreira, D.R., Wasserman, N.F. *et al.* (2014) Obesity-associated variants within FTO form long-range functional connections with IRX3. *Nature*, **507**, 371–375.

28. Zhao, Z., Tavoosidana, G., Sjölinder, M., Göndör, A., Mariano, P., Wang, S., Kanduri, C., Lezcano, M., Sandhu, K.S., Singh, U. *et al.* (2006) Circular chromosome conformation capture (4C) uncovers extensive networks of epigenetically regulated intra- and interchromosomal interactions. *Nat. Genet.*, **38**, 1341–1347.

29. van de Werken, H.J.G., Landan, G., Holwerda, S.J.B., Hoichman, M., Klous, P., Chachik, R., Splinter, E., Valdes-Quezada, C., Öz, Y., Bouwman, B.A.M. *et al.* (2012) Robust 4C-seq data analysis to screen for regulatory DNA interactions. *Nat. Methods*, **9**, 969–972.

30. Nora, E.P., Lajoie, B.R., Schulz, E.G., Giorgetti, L., Okamoto, I., Servant, N., Piolot, T., van Berkum, N.L., Meisig, J., Sedat, J. *et al.* (2012) Spatial partitioning of the regulatory landscape of the X-inactivation centre. *Nature*, **485**, 381–385.

31. Song, M., Pebworth, M.-P., Yang, X., Abnousi, A., Fan, C., Wen, J., Rosen, J.D., Choudhary, M.N.K., Cui, X., Jones, I.R. *et al.* (2020) Cell-type-specific 3D epigenomes in the developing human cortex. *Nature*, **587**, 644–649.

32. Ziller, M.J., Edri, R., Yaffe, Y., Donaghey, J., Pop, R., Mallard, W., Issner, R., Gifford, C.A., Goren, A., Xing, J. *et al.* (2015) Dissecting

neural differentiation regulatory networks through epigenetic footprinting. *Nature*, **518**, 355–359.

33. Stadler, M.B., Murr, R., Burger, L., Ivanek, R., Lienert, F., Schöler, A., van Nimwegen, E., Wirbelauer, C., Oakeley, E.J., Gaidatzis, D. *et al.* (2011) DNA-binding factors shape the mouse methylome at distal regulatory regions. *Nature*, **480**, 490–495.

34. The GTEx Consortium (2020) The GTEx Consortium atlas of genetic regulatory effects across human tissues. *Science*, **369**, 1318–1330.

35. Graybiel, A.M. (1990) Neurotransmitters and neuromodulators in the basal ganglia. *Trends Neurosci.*, **13**, 244–254.

36. Olsson, M., Björklund, A. and Campbell, K. (1998) Early specification of striatal projection neurons and interneuronal subtypes in the lateral and medial ganglionic eminence. *Neuroscience*, **84**, 867–876.

37. Wonders, C.P. and Anderson, S.A. (2006) The origin and specification of cortical interneurons. *Nat. Rev. Neurosci.*, **7**, 687–696.

38. Gilbert, L.A., Larson, M.H., Morsut, L., Liu, Z., Brar, G.A., Torres, S.E., Stern-Ginossar, N., Brandman, O., Whitehead, E.H., Doudna, J.A. *et al.* (2013) CRISPR-mediated modular RNA-guided regulation of transcription in eukaryotes. *Cell*, **154**, 442–451.

39. Thakore, P.I., D'Ippolito, A.M., Song, L., Safi, A., Shivakumar, N.K., Kabadi, A.M., Reddy, T.E., Crawford, G.E. and Gersbach, C.A. (2015) Highly specific epigenome editing by CRISPR-Cas9 repressors for silencing of distal regulatory elements. *Nat. Methods*, **12**, 1143–1149.

40. Fulco, C.P., Munschauer, M., Anyoha, R., Munson, G., Grossman, S.R., Perez, E.M., Kane, M., Cleary, B., Lander, E.S. and Engreitz, J.M. (2016) Systematic mapping of functional enhancer–promoter connections with CRISPR interference. *Science*, **354**, 769–773.

41. Robertson, K.D. (2005) DNA methylation and human disease. *Nat. Rev. Genet.*, **6**, 597–610.

42. Aran, D. and Hellman, A. (2013) DNA methylation of transcriptional enhancers and cancer predisposition. *Cell*, **154**, 11–13.

43. Yin, Y., Morgunova, E., Jolma, A., Kaasinen, E., Sahu, B., Khund-Sayeed, S., Das, P.K., Kivioja, T., Dave, K., Zhong, F. *et al.* (2017) Impact of cytosine methylation on DNA binding specificities of human transcription factors. *Science*, **356**, 502–+.

44. Reinhardt, P., Glatza, M., Hemmer, K., Tsytsyura, Y., Thiel, C.S., Höing, S., Moritz, S., Parga, J.A., Wagner, L., Bruder, J.M. *et al.* (2013) Derivation and expansion using only small molecules of human neural progenitors for neurodegenerative disease Modeling. *PLoS One*, **8**, e59252.

45. Buenrostro, J.D., Wu, B., Chang, H.Y. and Greenleaf, W.J. (2015) ATAC-seq: a method for assaying chromatin accessibility genome-wide. *Curr. Protoc. Mol. Biol.*, **109**, 21.29.1-21.29.9.

46. Langmead, B. and Salzberg, S.L. (2012) Fast gapped-read alignment with bowtie 2. *Nat. Methods*, **9**, 357–359.

47. Li, H., Handsaker, B., Wysoker, A., Fennell, T., Ruan, J., Homer, N., Marth, G., Abecasis, G., Durbin, R. and 1000 Genome Project Data Processing Subgroup (2009) The sequence alignment/map format and SAMtools. *Bioinforma. Oxf. Engl.*, **25**, 2078–2079.

48. Zhang, Y., Liu, T., Meyer, C.A., Eeckhoute, J., Johnson, D.S., Bernstein, B.E., Nusbaum, C., Myers, R.M., Brown, M., Li, W. *et al.* (2008) Model-based analysis of ChIP-Seq (MACS). *Genome Biol.*, **9**, R137.

49. Li, Q., Brown, J.B., Huang, H. and Bickel, P.J. (2011) Measuring reproducibility of high-throughput experiments. *Ann. Appl. Stat.*, **5**, 1752–1779.

50. Lopez-Delisle, L., Rabbani, L., Wolff, J., Bhardwaj, V., Backofen, B., Grüning, B., Ramírez, F. and Manke, T. (2021) pyGenomeTracks: reproducible plots for multivariate genomic datasets. *Bioinforma. Oxf. Engl.*, **37**, 422–423.

51. Preissl, S., Fang, R., Huang, H., Zhao, Y., Raviram, R., Gorkin, D.U., Zhang, Y., Sos, B.C., Afzal, V., Dickel, D.E. *et al.* (2018) Single-nucleus analysis of accessible chromatin in developing mouse forebrain reveals cell-type-specific transcriptional regulation. *Nat. Neurosci.*, **21**, 432–439.

52. Pliner, H.A., Packer, J.S., McFaline-Figueroa, J.L., Cusanovich, D.A., Daza, R.M., Aghamirzaie, D., Srivatsan, S., Qiu, X., Jackson, D., Minkina, A. *et al.* (2018) Cicero predicts cis-regulatory DNA interactions from single-cell chromatin accessibility data. *Mol. Cell*, **71**, 858–871.e8.

53. van de Werken, H.J.G., de Vree, P.J.P., Splinter, E., Holwerda, S.J.B., Klous, P., de Wit, E. and de Laat, W. (2012) 4C technology: protocols and data analysis. *Methods Enzymol.*, **513**, 89–112.

54. Bolger, A.M., Lohse, M. and Usadel, B. (2014) Trimmomatic: a flexible trimmer for Illumina sequence data. *Bioinformatics*, **30**, 2114–2120.

55. Walter, C., Schuetzmann, D., Rosenbauer, F. and Dugas, M. (2014) Basic4Cseq: an R/Bioconductor package for analyzing 4C-seq data. *Bioinformatics*, **30**, 3268–3269.

56. Aryee, M.J., Jaffe, A.E., Corrada-Bravo, H., Ladd-Acosta, C., Feinberg, A.P., Hansen, K.D. and Irizarry, R.A. (2014) Minfi: a flexible and comprehensive Bioconductor package for the analysis of Infinium DNA methylation microarrays. *Bioinformatics*, **30**, 1363–1369.

57. Ritchie, M.E., Phipson, B., Wu, D., Hu, Y., Law, C.W., Shi, W. and Smyth, G.K. (2015) Limma powers differential expression analyses for RNA-sequencing and microarray studies. *Nucleic Acids Res.*, **43**, e47–e47.

58. Wickham, H. (2016) ggplot2: elegant graphics for data analysis. In *ggplot2: Elegant Graphics for Data Analysis*. Springer-Verlag, New York, (2016).

59. Ramírez, F., Bhardwaj, V., Arrigoni, L., Lam, K.C., Grüning, B.A., Villaveces, J., Habermann, B., Akhtar, A. and Manke, T. (2018) High-resolution TADs reveal DNA sequences underlying genome organization in flies. *Nat. Commun.*, **9**, 189.

60. Ntalla, I., Weng, L.-C., Cartwright, J.H., Hall, A.W., Sveinbjornsson, G., Tucker, N.R., Choi, S.H., Chaffin, M.D., Roselli, C., Barnes, M.R. *et al.* (2020) Multi-ancestry GWAS of the electrocardiographic PR interval identifies 202 loci underlying cardiac conduction. *Nat. Commun.*, **11**.

61. Chen, M.-H., Raffield, L.M., Mousas, A., Sakaue, S., Huffman, J.E., Moscati, A., Trivedi, B., Jiang, T., Akbari, P., Vuckovic, D. *et al.* (2020) Trans-ethnic and ancestry-specific blood-cell genetics in 746,667 individuals from 5 global populations. *Cell*, **182**, 1198–1213.e14.

62. Pollard, K.S., Hubisz, M.J., Rosenbloom, K.R. and Siepel, A. (2010) Detection of nonneutral substitution rates on mammalian phylogenies. *Genome Res.*, **20**, 110–121.

63. Markenscoff-Papadimitriou, E., Whalen, S., Przytycki, P., Thomas, R., Binyameen, F., Nowakowski, T.J., Kriegstein, A.R., Sanders, S.J., State, M.W., Pollard, K.S. *et al.* (2020) A chromatin accessibility atlas of the developing human telencephalon. *Cell*, **182**, 754–769.e18.

64. Fullard, J.F., Hauberg, M.E., Bendl, J., Egervari, G., Cirnaru, M.-D., Reach, S.M., Motl, J., Ehrlich, M.E., Hurd, Y.L. and Roussos, P. (2018) An atlas of chromatin accessibility in the adult human brain. *Genome Res.*, **28**, 1243–1252.

65. ENCODE Project Consortium (2012) An integrated encyclopedia of DNA elements in the human genome. *Nature*, **489**, 57–74.

66. Davis, C.A., Hitz, B.C., Sloan, C.A., Chan, E.T., Davidson, J.M., Gabdank, I., Hilton, J.A., Jain, K., Baymuradov, U.K.,

Narayanan, A.K. *et al.* (2018) The Encyclopedia of DNA elements (ENCODE): data portal update. *Nucleic Acids Res.*, **46**, D794–D801.

67. Lindtner, S., Catta-Preta, R., Tian, H., Su-Feher, L., Price, J.D., Dickel, D.E., Greiner, V., Silberberg, S.N., McKinsey, G.L., McManus, M.T. *et al.* (2019) Genomic resolution of DLX-orchestrated transcriptional circuits driving development of forebrain GABAergic neurons. *Cell Rep.*, **28**, 2048–2063.e8.

68. Choi, W.-Y., Hwang, J.-H., Cho, A.-N., Lee, A.J., Jung, I., Cho, S.-W., Kim, L.K. and Kim, Y.-J. (2020) NEUROD1 intrinsically initiates differentiation of induced pluripotent stem cells into neural progenitor cells. *Mol. Cells*, **43**, 1011–1022.